Structural basis for functional cooperation between tandem helicase cassettes in Brr2-mediated remodeling of the spliceosome

Karine F. Santos[a,1], Sina Mozaffari Jovin[b,1], Gert Weber[a], Vladimir Pena[b], Reinhard Lührmann[b,2], and Markus C. Wahl[a,2]

[a]Fachbereich Biologie/Chemie/Pharmazie, Abteilung Strukturbiochemie, Freie Universität Berlin, D-14195 Berlin, Germany; and [b]Abteilung Zelluläre Biochemie, Max-Planck-Institut für Biophysikalische Chemie, D-37077 Göttingen, Germany

Edited by Thomas A. Steitz, Yale University, New Haven, CT, and approved September 11, 2012 (received for review May 11, 2012)

Assembly of a spliceosome, catalyzing precursor–messenger RNA splicing, involves multiple RNA–protein remodeling steps, driven by eight conserved DEXD/H-box RNA helicases. The 250-kDa Brr2 enzyme, which is essential for U4/U6 di-small nuclear ribonucleoprotein disruption during spliceosome catalytic activation and for spliceosome disassembly, is the only member of this group that is permanently associated with the spliceosome, thus requiring its faithful regulation. At the same time, Brr2 represents a unique subclass of superfamily 2 nucleic acid helicases, containing tandem helicase cassettes. Presently, the mechanistic and regulatory consequences of this unconventional architecture are unknown. Here we show that in human Brr2, two ring-like helicase cassettes intimately interact and functionally cooperate and how retinitis pigmentosa-linked Brr2 mutations interfere with the enzyme's function. Only the N-terminal cassette harbors ATPase and helicase activities in isolation. Comparison with other helicases and mutational analyses show how it threads single-stranded RNA, and structural features suggest how it can load onto an internal region of U4/U6 di-snRNA. Although the C-terminal cassette does not seem to engage RNA in the same fashion, it binds ATP and strongly stimulates the N-terminal helicase. Mutations at the cassette interface, in an intercassette linker or in the C-terminal ATP pocket, affect this cross-talk in diverse ways. Together, our results reveal the structural and functional interplay between two helicase cassettes in a tandem superfamily 2 enzyme and point to several sites through which Brr2 activity may be regulated.

pre-mRNA splicing | RNA helicase Brr2 | X-ray crystallography

Nucleotide triphosphate-dependent nucleic acid unwindases ("helicases") serve as motors and regulators of many biological macromolecular machines. Assembly of a spliceosome, catalyzing precursor–messenger RNA splicing, is a paradigmatic case that involves multiple RNA–protein remodeling steps, driven by eight conserved RNA helicases of the DEXD/H-box family (1). None of the spliceosome's small nuclear ribonucleoprotein (snRNP) subunits (U1, U2, U4, U5, and U6 in the major spliceosome) or its plethora of non-snRNP factors bear a preformed active center for splicing catalysis. Instead, profound compositional and conformational changes are required to convert an initial, inactive assembly to a catalytically competent spliceosome (2).

Catalytic activation involves the unwinding of the U4 and U6 snRNAs, which are extensively base-paired via two regions (stems 1 and 2) when delivered to the spliceosome in the framework of the U4/U6-U5 tri-snRNP. As the U5 snRNP protein, Brr2, unwinds U4/U6 duplexes in vitro (3, 4) and Brr2 mutations interfere with catalytic activation (5–7), the enzyme is thought to elicit these rearrangements. Brr2 already encounters its U4/U6 substrate in the U4/U6-U5 tri-snRNP, but U4/U6 dissociation must be delayed until splice sites have been reliably located during spliceosome assembly. Furthermore, unlike other spliceosomal helicases, Brr2 is stably associated with the spliceosome after its initial incorporation and is required again during spliceosome disassembly (8). Consequently, tight regulation of Brr2 is essential, but the underlying mechanisms are presently unknown. Moreover, as a member of the Ski2-like subfamily of superfamily (SF) 2 helicases, Brr2 is thought to translocate in a 3′ to 5′ direction on one of the substrate strands, but in the U4/U6 di-snRNP, both 3′ ends are sequestered in a stem–loop structure and/or are occluded by bound Sm/LSm proteins (9, 10). Thus, as for several other SF2 family members, it is presently unclear how Brr2 can engage its U4/U6 substrate. Brr2 is also of medical interest because mutations in the human enzyme have recently been linked to the RP33 form of autosomal-dominant retinitis pigmentosa (7, 11, 12).

Brr2 represents a unique subclass of nucleic acid helicases, containing tandem helicase cassettes expanded by Sec63 homology units, which also include the RNA helicase Slh1p involved in antiviral defense (13) and the ASCC3 DNA helicase of the activating signal cointegrator complex involved in genome maintenance (14). This unusual architecture of Brr2 is likely instrumental for its unique functions and may form the basis for the required regulation of the enzyme. However, unlike for single-cassette and oligomeric ring-like helicases, no structure of a member of the dual-cassette subclass is presently available. We, therefore, embarked on a combined structural and biochemical analysis of human (h) Brr2. Here we present the crystal structure of a protease-resistant, approximately 200-kDa portion of hBrr2 encompassing two ring-like helicase cassettes that interact extensively and form a functional unit. Concurrently, we show that the C-terminal cassette, although inactive on its own, strongly stimulates the N-terminal helicase. Mutational analyses pinpoint functionally important sites and suggest how Brr2 activity may be regulated on multiple levels.

Results

Crystal Structure of the hBrr2 Helicase Region. Although full-length hBrr2 could be produced recombinantly and purified (*SI Appendix*, Fig. S1*A*), it failed to crystallize. Using limited proteolysis, we identified a stable 200-kDa fragment encompassing both helicase cassettes (*SI Appendix*, Fig. S1*A*) that we refer to as Brr2 "helicase region" ($Brr2^{HR}$, residues 395–2,129). $hBrr2^{HR}$ was active in U4/U6 duplex unwinding (*SI Appendix*, Fig. S1*B*) and yielded a 2.7-Å-resolution crystal structure, in which we traced 1,723 residues (*SI Appendix*, *SI Results and Discussion*, Table S1, and Fig. S2).

The structure of $hBrr2^{HR}$ is compact with two structurally similar helicase cassettes [residues 463–1,288 and 1,310–2,125;

Author contributions: R.L. and M.C.W. designed research; K.F.S., S.M.J., G.W., and M.C.W. performed research; K.F.S., S.M.J., G.W., V.P., R.L., and M.C.W. analyzed data; and R.L. and M.C.W. wrote the paper.

The authors declare no conflict of interest.

This article is a PNAS Direct Submission.

Data deposition: The atomic coordinates and structure factors reported in this paper have been deposited in the Protein Data Bank, www.pdb.org [PDB ID codes 4F91 ($hBrr2^{HR}$), 4F92 ($hBrr2^{HR,S1087L}$), and 4F93 ($hBrr2^{HR,S1087L}$–Mg^{2+}–ATP complex)].

[1]K.F.S. and S.M.J. contributed equally to this work.

[2]To whom correspondence may be addressed. E-mail: mwahl@chemie.fu-berlin.de or reinhard.luehrmann@mpi-bpc.mpg.de.

This article contains supporting information online at www.pnas.org/lookup/suppl/doi:10.1073/pnas.1208098109/-/DCSupplemental.

Cα root-mean-square deviation (rmsd) 2.5 Å] closely associated via a 1,200-Å^2 interface (Fig. 1 and *SI Appendix*, Fig. S3). Both cassettes comprise two prototypical RecA-like ATPase domains followed by a winged helix (WH), a seven-helix bundle (HB), a helix–loop–helix (HLH), and an Ig-like (IG) domain (Fig. 1). The latter three domains constitute the Sec63 homology region and resemble the structure of isolated C-terminal Sec63 units

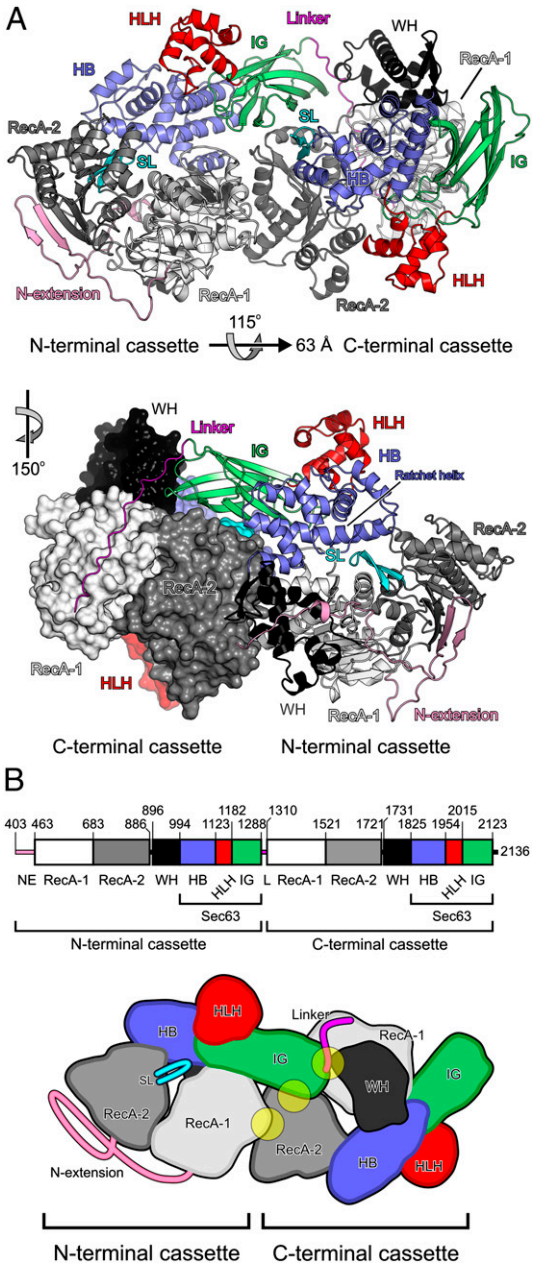

Fig. 1. Overall structure of hBrr2^{HR}. (*A Upper*) Ribbon plot of hBrr2^{HR}. N-terminal extension, pink; RecA-1, light gray; RecA-2, dark gray; WH, black; HB, blue; HLH, red; IG, green; linker, magenta; separator loop (SL), cyan. Symbols below the image indicate the relationship between the cassettes within hBrr2^{HR}. (*Lower*) Combined ribbon (N-terminal cassette) and surface (C-terminal cassette) plot showing the intercassette linker. Plot was rotated 150° counterclockwise as indicated. (*B*) Schematic representations of Brr2^{HR}. (*Upper*) Domain borders. (*Lower*) A 2D scheme of Brr2^{HR}. Intercassette contacts between the N-terminal IG domain and the C-terminal RecA-2 and WH domains and between the N-terminal RecA-1 and the C-terminal RecA-2 domains are indicated by semitransparent yellow circles.

from yeast (15, 16) and human Brr2 [Protein Data Bank (PDB) ID code 2Q0Z]. Sixty conserved residues preceding the first RecA domain (*SI Appendix*, Fig. S4) tightly encircle the N-terminal cassette (Fig. 1*A*). The reduction in helicase activity observed upon deletion of this N-terminal expansion (*SI Appendix*, *SI Results and Discussion* and Fig. S1*B*) suggests that it supports a productive domain organization. An extended 20-residue intercassette linker (residues 1,289–1,309) following the N-terminal IG domain runs snugly along one entire flank of the C-terminal RecA-1 domain (Fig. 1*A*). The N-terminal IG domain thereby fits squarely between the C-terminal RecA-2 and WH domains. An additional intercassette contact area ensues between the N-terminal RecA-1 and WH domains and the C-terminal RecA-2 domain (Fig. 1*A* and *SI Appendix*, Fig. S3). The extensive contacts between the two cassettes suggest that they form a functional unit.

Organization of the Individual Helicase Cassettes. In both Brr2 cassettes, the two RecA domains and the HB domain form the bottom and top, respectively, of a central tunnel (Fig. 2*A*). The WH domain constitutes one side of the tunnel and fastens the first RecA domain to the HB domain. On the other side, the second RecA and the HB domain approach (N-terminal cassette) or contact (C-terminal cassette) each other (Fig. 2*A*). A prominent loop of the RecA-2 domain extends across the tunnel entry toward a long scaffolding helix of the HB domain (Fig. 2*A*). Equivalents of these elements have been suggested to constitute a strand separation device and a ratchet, respectively, in other SF2 proteins (17). Although direct evidence for a ratchet function of the HB scaffolding helix is missing, we refer to it as the "ratchet helix" in keeping with previous nomenclature (7, 16). In the Sec63 units, the IG domain is wedged between the HB and HLH modules, which in turn do not directly contact each other. Our structure shows that the individual Brr2 cassettes both resemble the complete SF2 DNA helicase Hel308 (17) expanded by an IG domain. As in Hel308, the circular domain arrangement in both hBrr2^{HR} cassettes leads to the clustering of conserved ATPase/helicase motifs, known to bind and hydrolyze nucleotide triphosphates and to bind nucleic acids (*SI Appendix*, Fig. S5*A*).

Activities of the Cassettes. Previous genetic analyses have shown that the ATPase and helicase activities of the N-terminal cassette of Brr2 are required for splicing, whereas putatively inactivating mutations were tolerated at the C-terminal cassette (6), suggesting that the C-terminal cassette may not be an active ATPase or helicase. To directly test this notion, we produced soluble fragments encompassing solely the N- or C-terminal cassette (hBrr2^{NC}, residues 395–1,324; hBrr2^{CC}, residues 1,282–2,136). Although hBrr2^{NC} retained ATPase and U4/U6 di-snRNA unwinding activities, hBrr2^{CC} was entirely inactive as an ATPase or helicase (Fig. 2 *B* and *C*). However, U4/U6 di-snRNA unwinding by hBrr2^{NC} was markedly reduced compared with the dual-cassette construct, hBrr2^{HR} (Fig. 2 *C* and *D*). hBrr2^{NC} and hBrr2^{HR} also exhibited differences in the unwinding of a simple model duplex bearing a single-stranded 3′ overhang (Fig. 2*D*). These results show that the N-terminal cassette harbors the helicase activity of Brr2, whereas the C-terminal cassette acts as an intramolecular cofactor.

The C-terminal cassette of Brr2 contains a number of noncanonical residues in its ATPase/helicase motifs (5, 18). To investigate why it is inactive as an ATPase and whether it may nevertheless still bind ATP, we attempted to determine structures of Brr2 in complex with nucleotides or nucleotide analogs. Cocrystallization attempts failed because of the high salt concentrations required by hBrr2^{HR}. To soak nucleotides into the crystals at lower ionic strength, hBrr2^{HR} crystals were stabilized by cross-linking. Soaking of cross-linked crystals with ATP or analogs yielded the same results—nucleotides bound at both cassettes without significant conformational changes and in a manner incompatible with ATP hydrolysis (Fig. 3).

Irrespective of the nucleotide used, an ADP moiety, presumably originating from contamination in the nucleotide preparations, was bound at the N-terminal cassette (Fig. 3*A*),

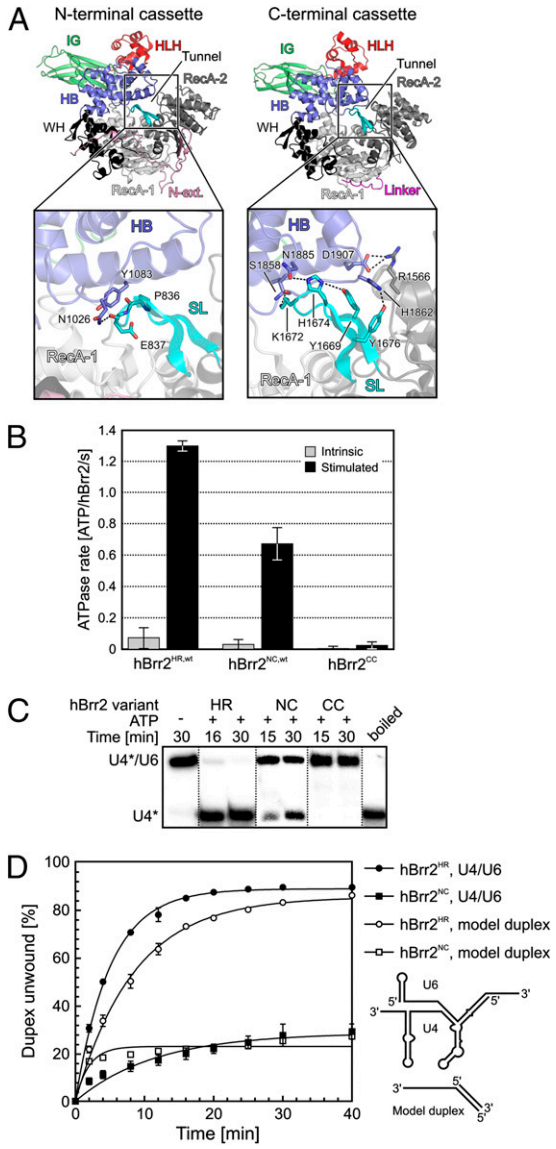

Fig. 2. Organization and activities of the individual cassettes. (*A*) Ribbon plots of N-terminal (*Left*) and C-terminal (*Right*) cassettes with expanded views on the domain closure and contacts between the separator loops and the ratchet helices. Interacting residues are shown as sticks and colored by atom type (carbon, as the respective structural element; nitrogen, blue; oxygen, red). Dashed lines, hydrogen bonds or salt bridges. The view of the N-terminal cassette is the same as in Fig. 1*A Lower*. The C-terminal cassette is shown in an identical orientation. (*B*) Intrinsic (gray bars) and RNA-stimulated (black bars) ATPase activities of $Brr2^{HR}$ compared with the individual cassettes. Error bars represent SEMs for three independent measurements. (*C*) Unwinding of U4/U6 di-snRNA by $Brr2^{HR}$ and the isolated N-terminal cassette and lack of helicase activity in the isolated C-terminal cassette. Lanes were compiled from three identically processed gels. (*D*) Unwinding time courses comparing the activities of $hBrr2^{HR}$ and $hBrr2^{NC}$ toward U4/U6 and a model duplex with a single-stranded 3′ overhang. Error bars represent SEMs for two independent measurements. Apparent unwinding rate constants (k_u) and amplitudes (A): $hBrr2^{HR,wt}$/U4/U6, $k_u = 0.200 \pm 0.006$ min^{-1}, $A = 88.9 \pm 0.6\%$; $hBrr2^{HR,wt}$/model duplex, $k_u = 0.118 \pm 0.006$ min^{-1}, $A = 85.5 \pm 1.2\%$; $hBrr2^{NC,wt}$/U4/U6, $k_u = 0.087 \pm 0.016$ min^{-1}, $A = 28.6 \pm 1.9\%$; $hBrr2^{NC,wt}$/model duplex, $k_u = 0.521 \pm 0.13$ min^{-1}, $A = 22.9 \pm 0.9\%$.

whereas Mg^{2+}–ATP (or analog) was bound at the C-terminal cassette (Fig. 3*B*). In both cassettes, the nucleotide was primarily contacted by motifs from the first RecA domain and lacked interactions with RecA-2, which are required for ATP hydrolysis. Upon RNA binding, the N-terminal cassette is expected to undergo conformational changes that would allow ATP hydrolysis. In contrast, a similar rearrangement seems to be hindered at the C-terminal cassette due to a contact between the noncanonical N1692 (motif VI) and G1353 (motif I) from the first RecA domain (Fig. 3*B*; *SI Appendix*, *SI Results and Discussion*).

Effects of Retinitis Pigmentosa-Linked hBrr2 Mutations. A number of mutations in Brr2 have been linked to the RP33 form of retinitis pigmentosa (7, 11, 12). To gain insights into the underlying disease mechanisms, we located the affected residues in the $hBrr2^{HR}$ structure. One set of affected residues lies in the connection between the N-terminal RecA domains (R681C, R681H, and V683L) and in the first β-strand of the RecA-2 domain (Y689C), where they establish interdomain contacts and stabilize domain folds (*SI Appendix*, Fig. S6 *A* and *B*). Another set of mutations maps to the ratchet helix of the N-terminal HB domain (S1087L, R1090L; *SI Appendix*, Fig. S6 *C–E*) and corresponding changes in yeast (y) Brr2 were detrimental to U4/U6 unwinding and splicing (7, 15, 16). R1090 (conserved as R1107 in yBrr2) extends from the underside of the ratchet helix (*SI Appendix*, Fig. S6*C*) and is thus likely important for interaction with RNA. Because S1087 is an asparagine in yBrr2 (N1104), we directly tested the consequences of a leucine at this position in the disease-relevant human protein. $hBrr2^{HR,S1087L}$ exhibited decreased RNA binding and reduced ATPase and helicase activities compared with the wild-type (wt) variant (*SI Appendix*, Fig. S7*A*). The crystal structure of $hBrr2^{HR,S1087L}$ at 2.65-Å resolution (*SI Appendix*, Table S1) revealed no significant conformational changes compared with $hBrr2^{HR}$ (Cα rmsd 0.4 Å) except that a leucine at position 1,087 interacts more intimately with a neighboring hydrophobic/aromatic cluster (*SI Appendix*, Fig. S6

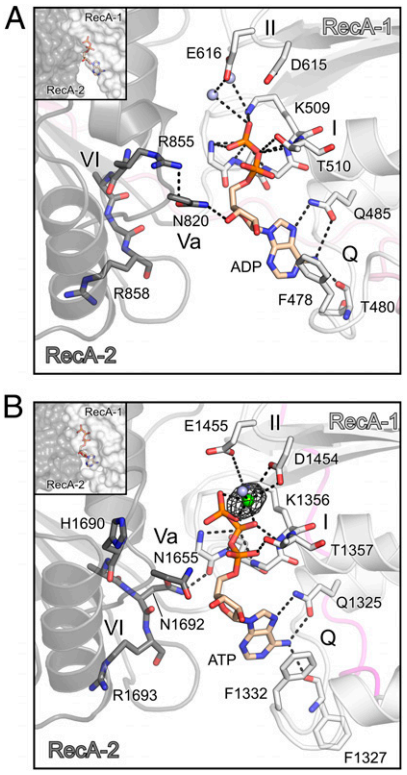

Fig. 3. Nucleotide binding. Close-up views of the ATP pockets of the N-terminal (*A*) and C-terminal (*B*) cassettes. Nucleotides and selected residues are shown as sticks and colored by atom type (carbon ATP, beige; phosphorus, orange). Blue spheres, water molecules; green sphere, Mn^{2+} ion. Q and Roman numerals, conserved motifs. Gray mesh in *B* indicates anomalous-difference electron density contoured at the 4σ level.

D and *E*). Therefore, S1087L abrogates functionally important S1087–RNA contacts and/or counteracts conformational changes in the ratchet helix, which have been suggested in related DEAH helicases (19). Because S1087L has no discernible effect on the folding of Brr2, it is likely that this and perhaps other RP33-linked Brr2 variants are incorporated into spliceosomes in vivo. Thus, our findings support the slow-down of spliceosome catalytic activation through impairment of hBrr2 activity as a RP33 disease principle. In addition to the above disease-related mutations, our hBrr2^{HR} structure also offers explanations for the malfunction of several other previously investigated Brr2 alleles (*SI Appendix*, *SI Results and Discussion* and Fig. S8).

RNA Accommodation and Loading. So far, we failed to cocrystallize hBrr2^{HR} in complex with RNA. To investigate whether and how the C-terminal cassette may contribute to substrate binding, we modeled RNA at the active N-terminal cassette in analogy to nucleic acid binding by the related SF2 DNA helicase Hel308 (17) and the SF2 RNA helicase Mtr4 (20). In the model, one RNA strand is threaded through the central tunnel of the N-terminal cassette, running across the conserved RNA-binding motifs of the RecA domains, alongside the separator loop, and beneath the ratchet helix of the HB domain (*SI Appendix*, Fig. S9 *A* and *B*). The model suggested that upon emergence from the N-terminal tunnel, the RNA strand may exit via a positively charged surface on the N-terminal HLH domain (*SI Appendix*, Fig. S9*B*, path 1) or continue in the direction of the putative separator loop of the C-terminal cassette (*SI Appendix*, Fig. S9*B*, path 2). We resorted to a mutational strategy to distinguish between these alternatives. This and the following mutational analyses were based on the RP33-linked S1087L variant of Brr2^{HR} (see above; *SI Appendix*, *SI Results and Discussion*, and Fig. S7).

Mutation of two positively charged residues on the surface of the N-terminal HLH domain, which do not directly contact other hBrr2^{HR} residues (RK1133-4EE; Fig. 4*A*), was associated with enhanced ATPase activity (Fig. 4*E*, lane 2), whereas both U4/U6 unwinding (Fig. 4*F*, lane 4) and binding of an RNA duplex with a 31-residue 3′ overhang (Fig. 4*H*) were strongly diminished. Conversely, replacement of the putative separator loop in the C-terminal cassette (residues 1,668–1,677) by a single serine had virtually no effect on hBrr2^{HR,S1087L} ATPase (Fig. 4*E*, lane 3) or U4/U6 unwinding activities (Fig. 4 *F*, lane 5, and *G*) and did not reduce binding of the model duplex (Fig. 4*H*), in stark contrast to the essential nature of the corresponding element in the N-terminal cassette of yBrr2 (15, 16). These findings support the idea that an unwound RNA strand traverses the N-terminal HLH domain, as seen for DNA in Hel308 (17), and is guided away from the C-terminal cassette. Consistently, part of the rim and inner walls of the tunnel at the C-terminal cassette are negatively charged, counteracting RNA binding (*SI Appendix*, Fig. S5*B*).

In the U4/U6 di-snRNP, the 3′ ends of U4 and U6 snRNA are occluded by secondary structures and/or bound proteins (9, 10) and are thus unavailable for Brr2 binding. Psoralen cross-linking of the RNA network in the minor spliceosome indicated that U4atac/U6atac stem 1 (equivalent to U4/U6 stem 1 in the major spliceosome) is unwound before stem 2 during catalytic activation, implying that Brr2 translocates on U4 (U4atac) snRNA in 3′ to 5′ direction (21). We suggest that Brr2 circumvents the sequestered 3′ end of U4 (U4atac) snRNA by intermittent opening of its N-terminal RecA-2 and HB domains and loading onto the internal single-stranded U4 (U4atac) snRNA region immediately downstream of stem 1. N-terminal cassette opening appears feasible considering the limited interactions between the RecA-2 and HB domains (Fig. 2*A*) and in light of the crystallographic B-factor distribution, showing that the tip of the N-terminal RecA-2 domain is one of the most flexible portions of the hBrr2^{HR} crystal structure (*SI Appendix*, Fig. S9*C*).

Functional Communication Between the Helicase Cassettes. We next asked which intercassette contacts or connections are important for the observed cooperation of the cassettes. Single alanine substitutions in contacts between the N-terminal RecA-1 or WH domains and the C-terminal RecA-2 domain (R603A, R637A, K1544A, H1548A and T1578A; Fig. 4*B*) led to changes in ATPase activity (Fig. 4*E*, lanes 4–8), and the majority of mutations strongly diminished helicase activity (Fig. 4 *F*, lanes 6–10, and *G*). None of the mutated residues belongs to the canonical ATPase/helicase motifs of either cassette, suggesting that all phenotypes were due to disturbed cassette interactions. Indeed, RNA binding by the K1544A mutant was essentially unchanged (Fig. 4*H*).

Mutations of residues in the intercassette linker that contact the N-terminal IG (ILP1290-2AAA; Fig. 4*C*) or C-terminal RecA-1 domain (LPV1307-9AAA; Fig. 4*D*) had similarly severe effects on N-terminal ATPase (Fig. 4*E*, lanes 9 and 12) and helicase activity (Fig. 4*F*, lanes 11 and 14). Furthermore, mutating a reciprocal contact from the N-terminal IG domain to the linker (R1195A; Fig. 4*C*) also led to defective duplex unwinding (Fig. 4 *E*, lane 10, and *F*, lane 12). Strikingly, mutation of a conserved proline motif in the center of the linker (PPP1296-8AAA; Fig. 4*C*), which does not directly contact the bulk of hBrr2^{HR}, reduced ATPase (Fig. 4*E*, lane 11) but strongly upregulated helicase activity (Fig. 4 *F*, lane 13, and *G*).

To investigate whether nucleotide binding at the C-terminal cassette influences the N-terminal helicase, we introduced changes in the C-terminal ATP pocket of hBrr2^{HR} designed to interfere with nucleotide accommodation (GK1355-6QE; Fig. 3*B*). Although ATPase activity was only mildly affected (Fig. 4*E*, lane 13), helicase activity was strongly reduced in this mutant (Fig. 4*F*, lane 15).

Discussion

We have presented the crystal structure of the entire Brr2 helicase region, revealing how two helicase cassettes are arranged with respect to each other in a tandem SF2 enzyme. Guided by this structure, we have interrogated the mechanism and regulation of the enzyme by mutational analyses, delineating a number of unique regulatory features and providing a solid framework on which to interpret mechanistic studies.

Pseudoenzyme Domain as an Intramolecular Helicase Cofactor. Most enzyme families include inactive members, which often emerged due to gene duplication and subsequent accumulation of inactivating mutations (22). Evolutionary conservation suggests that such pseudoenzymes are functionally important; however, in most cases, their functions are unknown (22). Here, we have shown that the C-terminal cassette of Brr2 is a pseudohelicase that has been converted into an intramolecular regulator of a neighboring, similarly structured, active helicase. These findings are in agreement with noncanonical ATPase/helicase motifs in the C-terminal cassette (5, 18) and with previous genetics analyses (6). However, our results additionally show that the C-terminal cassette has retained its ATP binding activity but has specifically lost its ability to hydrolyze the nucleotide. Furthermore, apart from the previously identified active site mutations, the C-terminal cassette exhibits an increased barrier to adopt a hydrolytic conformation (Fig. 3*B*; *SI Appendix*, *SI Results and Discussion*).

Modeling and mutational analyses suggest that the C-terminal cassette also does not contribute RNA contacts required for U4/U6 unwinding. Indirectly supporting this notion, differences in the N-terminal helicase activity due to the presence of the C-terminal cassette were not only observed with U4/U6 di-snRNA as a substrate but also with a simple model duplex. Thus, the C-terminal cassette does not appear to rely on specific sequences or structures of U4/U6 for influencing the N-terminal active cassette.

Possible Mechanisms for Regulation Through the C-Terminal Cassette. Our mutational studies show that direct intercassette contacts are essential for cassette communication. Because of their large contact area, the cassettes most likely mutually stabilize the conformational states they adopt in the apo form of hBrr2^{HR}. Because we do not observe any significant conformational changes in the nucleotide-bound states (possibly due to cross-linking) and because our nucleotide preparations obviously

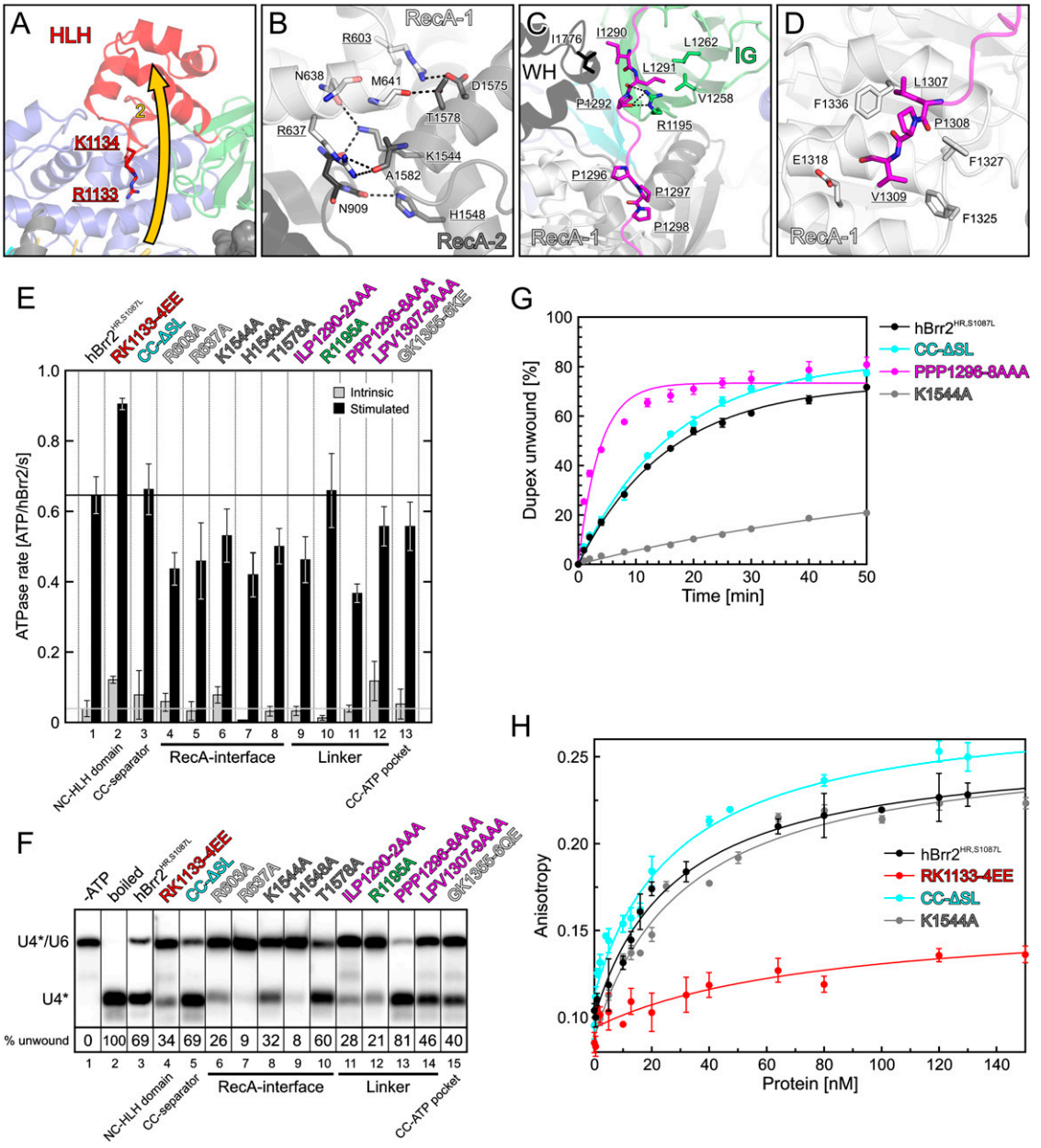

Fig. 4. Mutational analysis of hBrr2^{HR}. All proteins investigated carry the S1087L mutation in addition to the indicated changes. (*A*) Close-up view on the N-terminal HLH domain. R1133 and K1134 comprise bona fide RNA contact sites. Gold arrow, putative path of the RNA. Image is in the same orientation as in Fig. 1*A Upper*. (*B*) Contacts between the N-terminal RecA-1 and the C-terminal RecA-2 domain. Image is rotated 90° about the horizontal axis (top to back) compared with Fig. 1*A Upper*. (*C*) Upper portion of the linker. Image is rotated 30° about the horizontal axis (top to front) compared with Fig. 1*A Lower*. (*D*) Lower portion of the linker. Image is rotated 30° about the horizontal axis (top to back) compared with Fig. 1*A Lower*. Mutated residues in *A–D* are underlined. (*E*) Intrinsic (gray bars) and U4/U6-stimulated (black bars) rates of ATP hydrolysis of the hBrr2^{HR,S1087L} variants indicated. NC, N-terminal cassette; CC, C-terminal cassette; CC-ΔSL, replacement of the C-terminal separator loop by a single serine. Error bars represent SEMs for three independent measurements. (*F*) Single point unwinding assays comparing the hBrr2^{HR,S1087L} variants indicated above the gel. Quantification (percent unwound after 50 min) is shown below the image. Lanes were compiled from two identically processed gels. (*G*) Unwinding time courses of selected hBrr2^{HR,S1087L} variants. Apparent unwinding rate constants (k_u) and amplitudes (*A*): hBrr2^{HR,S1087L}, $k_u = 0.064 \pm 0.003$ min^{-1}, $A = 73.0 \pm 1.2\%$; hBrr2$^{HR,CC\text{-}\Delta SL}$, $k_u = 0.062 \pm 0.003$ min^{-1}, $A = 82.4 \pm 1.8\%$; hBrr2$^{HR,PPP1296\text{-}8AAA}$, $k_u = 0.27 \pm 0.04$ min^{-1}, $A = 73.3 \pm 2.2\%$; hBrr2^{HR,K1544A}, $k_u = 0.015 \pm 0.003$ min^{-1}, $A = 39.3 \pm 6.5\%$. Error bars represent SEMs for two independent measurements. (*H*) RNA binding by the indicated hBrr2^{HR,S1087L} variants measured by fluorescence polarization. Error bars represent SEMs for three independent measurements. K_d hBrr2^{HR,S1087L}, 28.5 ± 3.8 nM; K_d hBrr2$^{HR,RK133\text{-}4EE}$, not determined; K_d hBrr2$^{HR,CC\text{-}\Delta SL}$, 31.0 ± 6.3 nM; K_d hBrr2^{HR,K1544A}, 35.0 ± 7.2 nM. Mutant labels and curves in *E–H* are colored according to their domains or elements (hBrr2^{HR,S1087L} reference, black).

contained both ATP (or analog) and ADP, the outcome of our soaking experiments indicates which nucleotide is preferentially bound by the apo form conformations (ADP at the N-terminal cassette, Mg^{2+}–ATP at the C-terminal cassette). ADP binding at the N-terminal cassette suggests that the C-terminal cassette stabilizes the state after ATP hydrolysis and phosphate release. Thus, one function of the C-terminal cassette may be to drive ATP hydrolysis and/or phosphate release by the N-terminal cassette, thereby facilitating associated changes in nucleic acid binding. In agreement with this interpretation, the N-terminal ATPase activity is indeed enhanced in the presence of the C-terminal cassette (Fig. 2*B*).

The C-terminal cassette preferentially binds Mg^{2+}–ATP in the presence of the N-terminal cassette. Because the adoption of the hydrolytic conformation is hindered at the C-terminal cassette, it seems to be conformationally more restricted than the N-terminal cassette and may remain stably associated with the nucleotide, rather than cycling between nucleotide-bound and free states during RNA unwinding. The function of the nucleotide at the C-terminal cassette, therefore, may be to rigidify its structure and allow it to act as a scaffold on which the N-terminal cassette could efficiently undergo conformational changes required for duplex unwinding.

The C-terminal cassette may also exploit intercassette contacts to directly influence the positioning of active site domains in the N-terminal cassette. Interactions between the HLH and HB domains are important for duplex unwinding in the related Hel308 (23). In Brr2, the N-terminal IG domain intervenes between the HLH and HB domains and is connected to the upper part of the intercassette linker (Figs. 1*A* and 4*C*). Mutations in the linker affect $Brr2^{HR}$ activity both negatively and positively. It is conceivable that different functional states (such as ATP, ADP $+P_i$, and ADP-bound) are associated with different relative orientations of the cassettes and that such conformational changes may be transmitted via the linker and the IG domain to the N-terminal HLH and HB domains.

Potential for Regulation from a Distance. Mutations that interfere with ATP binding at the C-terminal cassette—i.e., remote from the N-terminal active site and remote from the cassette interface—also exhibit strong effects on the N-terminal helicase (Fig. 4*F*). This observation demonstrates that, in principle, ligand binding at the C-terminal cassette can be sensed by the N-terminal helicase. Although we presently cannot trace this long-range communication on the atomic level, it is likely also conducted through the direct intercassette RecA or linker contacts discussed above.

A number of proteins essential for different steps of splicing interact with the C-terminal cassette of Brr2 (24, 25). The ability of the C-terminal cassette to transmit signals to the N-terminal cassette suggests that these proteins may not merely use the C-terminal cassette as a passive landing pad but also to influence the N-terminal cassette from a distance. The observation that, although many mutations reduced Brr2 helicase activity, one variant (PPP1296–8AAA in the linker) exhibited significantly enhanced unwinding activity indicates that interacting factors may either down- or up-regulate Brr2. Sequentially binding proteins may thus switch the enzyme on or off as required during particular phases of the splicing process.

The above principles offer one solution to the intriguing problem of how a large number of factors can influence alternative splicing. Several of these proteins may directly or indirectly target the expanded surface provided by the C-terminal cassette to modulate Brr2 activity, which would affect splicing kinetics and consequently the choice or proofreading of (alternative) splice sites. Analogous kinetic switches, influencing splice site choice via the modulation of U1 snRNP interaction with 5′-splice sites, have recently been uncovered (26).

Materials and Methods

Recombinant proteins were expressed in insect cell culture and purified by chromatographic techniques. Crystallization experiments were performed by sitting drop vapor diffusion, and diffraction data were collected at cryogenic temperatures at synchrotron beamlines. For nucleotide soaking, crystals were stabilized by cross-linking and transferred into low-salt buffer. Crystal structures were solved by using the multiple isomorphous replacement with anomalous scattering and molecular replacement strategies. Molecular models were built manually and refined by standard protocols. RNAs were produced by chemical synthesis or by in vitro transcription using T7 RNA polymerase. RNA binding was analyzed by fluorescence polarization, ATPase activity of hBrr2 variants was analyzed by using a malachite dye-based assay. RNA unwinding by hBrr2 variants was analyzed with 5′-[^{32}P]-labeled RNA duplexes. Detailed materials and methods can be found in *SI Appendix, SI Materials and Methods*.

ACKNOWLEDGMENTS. We thank Imre Berger (Grenoble, France) for support in baculovirus-based expression; Gleb Bourenkov and Thomas Schneider for support at beamline P14 of PETRA III (Deutsches Elektronen Synchrotron, Hamburg, Germany); and the staff of beamline PXII (Protein Crystallography Beamline II) of the Swiss Light Source (Paul Scherrer Institute). We accessed beamlines of the BESSY II (Berliner Elektronenspeicherring-Gesellschaft für Synchrotronstrahlung II) storage ring (Berlin, Germany) via the Joint Berlin MX-Laboratory sponsored by the Helmholtz Zentrum Berlin für Materialien und Energie, the Freie Universität Berlin, the Humboldt-Universität zu Berlin, the Max-Delbrück Centrum, and the Leibniz-Institut für Molekulare Pharmakologie. This work was supported by Deutsche Forschungsgemeinschaft Grants SFB 740 (to M.C.W.) and SFB 860 (to R.L.); the Seventh Framework Programme of the European Commission Infrastructure for Protein Production Platforms (P-CUBE) project, Freie Universität Berlin, and Max-Planck-Gesellschaft.

1. Staley JP, Guthrie C (1998) Mechanical devices of the spliceosome: Motors, clocks, springs, and things. *Cell* 92:315–326.
2. Wahl MC, Will CL, Lührmann R (2009) The spliceosome: Design principles of a dynamic RNP machine. *Cell* 136:701–718.
3. Laggerbauer B, Achsel T, Lührmann R (1998) The human U5-200kD DEXH-box protein unwinds U4/U6 RNA duplices in vitro. *Proc Natl Acad Sci USA* 95:4188–4192.
4. Raghunathan PL, Guthrie C (1998) RNA unwinding in U4/U6 snRNPs requires ATP hydrolysis and the DEIH-box splicing factor Brr2. *Curr Biol* 8:847–855.
5. Noble SM, Guthrie C (1996) Identification of novel genes required for yeast pre-mRNA splicing by means of cold-sensitive mutations. *Genetics* 143:67–80.
6. Kim DH, Rossi JJ (1999) The first ATPase domain of the yeast 246-kDa protein is required for in vivo unwinding of the U4/U6 duplex. *RNA* 5:959–971.
7. Zhao C, et al. (2009) Autosomal-dominant retinitis pigmentosa caused by a mutation in SNRNP200, a gene required for unwinding of U4/U6 snRNAs. *Am J Hum Genet* 85:617–627.
8. Small EC, Leggett SR, Winans AA, Staley JP (2006) The EF-G-like GTPase Snu114p regulates spliceosome dynamics mediated by Brr2p, a DExD/H box ATPase. *Mol Cell* 23:389–399.
9. Achsel T, et al. (1999) A doughnut-shaped heteromer of human Sm-like proteins binds to the 3′-end of U6 snRNA, thereby facilitating U4/U6 duplex formation in vitro. *EMBO J* 18:5789–5802.
10. Leung AK, Nagai K, Li J (2011) Structure of the spliceosomal U4 snRNP core domain and its implication for snRNP biogenesis. *Nature* 473:536–539.
11. Li N, Mei H, MacDonald IM, Jiao X, Hejtmancik JF (2010) Mutations in ASCC3L1 on 2q11.2 are associated with autosomal dominant retinitis pigmentosa in a Chinese family. *Invest Ophthalmol Vis Sci* 51:1036–1043.
12. Benaglio P, et al. (2011) Next generation sequencing of pooled samples reveals new SNRNP200 mutations associated with retinitis pigmentosa. *Hum Mutat* 32: E2246–E2258.
13. Martegani E, et al. (1997) Identification of gene encoding a putative RNA-helicase, homologous to SKI2, in chromosome VII of Saccharomyces cerevisiae. *Yeast* 13:391–397.
14. Dango S, et al. (2011) DNA unwinding by ASCC3 helicase is coupled to ALKBH3-dependent DNA alkylation repair and cancer cell proliferation. *Mol Cell* 44:373–384.
15. Pena V, et al. (2009) Common design principles in the spliceosomal RNA helicase Brr2 and in the Hel308 DNA helicase. *Mol Cell* 35:454–466.
16. Zhang L, et al. (2009) Structural evidence for consecutive Hel308-like modules in the spliceosomal ATPase Brr2. *Nat Struct Mol Biol* 16:731–739.
17. Büttner K, Nehring S, Hopfner KP (2007) Structural basis for DNA duplex separation by a superfamily-2 helicase. *Nat Struct Mol Biol* 14:647–652.
18. Lauber J, et al. (1996) The HeLa 200 kDa U5 snRNP-specific protein and its homologue in Saccharomyces cerevisiae are members of the DEXH-box protein family of putative RNA helicases. *EMBO J* 15:4001–4015.
19. Walbott H, et al. (2010) Prp43p contains a processive helicase structural architecture with a specific regulatory domain. *EMBO J* 29:2194–2204.
20. Weir JR, Bonneau F, Hentschel J, Conti E (2010) Structural analysis reveals the characteristic features of Mtr4, a DExH helicase involved in nuclear RNA processing and surveillance. *Proc Natl Acad Sci USA* 107:12139–12144.
21. Frilander MJ, Steitz JA (2001) Dynamic exchanges of RNA interactions leading to catalytic core formation in the U12-dependent spliceosome. *Mol Cell* 7:217–226.
22. Adrain C, Freeman M (2012) New lives for old: Evolution of pseudoenzyme function illustrated by iRhoms. *Nat Rev Mol Cell Biol* 13:489–498.
23. Woodman IL, Briggs GS, Bolt EL (2007) Archaeal Hel308 domain V couples DNA binding to ATP hydrolysis and positions DNA for unwinding over the helicase ratchet. *J Mol Biol* 374:1139–1144.
24. van Nues RW, Beggs JD (2001) Functional contacts with a range of splicing proteins suggest a central role for Brr2p in the dynamic control of the order of events in spliceosomes of Saccharomyces cerevisiae. *Genetics* 157:1451–1467.
25. Liu S, Rauhut R, Vornlocher HP, Lührmann R (2006) The network of protein-protein interactions within the human U4/U6.U5 tri-snRNP. *RNA* 12:1418–1430.
26. Yu Y, et al. (2008) Dynamic regulation of alternative splicing by silencers that modulate 5′ splice site competition. *Cell* 135:1224–1236.